JOURNAL OF MATERIALS SCIENCE 20 (1985) 3329 - 3338

Mechanisms of stress-corrosion cracking and liquid-metal embrittlement in Al–Zn–Mg bicrystals

S. P. LYNCH
Aeronautical Research Laboratories, Defence Science and Technology Organisation, Department of Defence, Melbourne, Australia

Metallographic and fractographic studies of intercrystalline fracture in high-purity Al–6Zn–3Mg bicrystals in inert, liquid metal, and water environments are described. The effects of variations in grain-boundary microstructure on fracture and the effects of cathodically charging specimens with hydrogen prior to testing in inert environments were also investigated. Mechanisms of liquid-metal embrittlement, stress-corrosion cracking and pre-exposure embrittlement are discussed in the light of these results. The observations suggest that liquid-metal embrittlement and stress-corrosion cracking generally occur by a plastic-flow/microvoid-coalescence process that is more localized than that which occurs in inert environments. It is proposed that adsorbed liquid metal or hydrogen atoms weaken interatomic bonds at crack tips, thereby facilitating the nucleation of dislocations and promoting the coalescence of cracks with voids.

1. Introduction

It is now widely accepted [1–7] that intercrystalline cracking in high-purity and commercial Al–Zn–Mg alloys can be facilitated by the presence of hydrogen at grain boundaries. This acceptance is based largely on the phenomenon of "pre-exposure embrittlement" [2, 8, 9], namely observations that (a) pre-exposure of specimens to aqueous and moist environments prior to testing in inert environments at slow strain rates can decrease ductility and produce "brittle" intercrystalline fractures, (b) the ductility of pre-exposed specimens can be at least partially restored by re-heat treatment or by storing specimens in a vacuum prior to testing, and (c) hydrogen is evolved during deformation and fracture of pre-exposed specimens. Bubbles, presumably containing hydrogen, have also been observed along grain boundaries after electron irradiation [4].

Intercrystalline stress-corrosion cracking (SCC) is also often attributed to the effects of hydrogen at grain boundaries since (a) fracture surfaces produced by SCC in moist and aqueous environments are similar to those observed for pre-exposed specimens [8, 9], (b) SCC occurs in moist air at low relative humidities (i.e. in the absence of a liquid electrolyte), and hence a dissolution mechanism – the main alternative to a hydrogen-embrittlement mechanism – cannot be applicable [10], (c) SCC is promoted by the presence of a hydrostatic stress which favours the concentration of hydrogen ahead of cracks [3, 11], and (d) there is evidence, e.g. striations on otherwise smooth fracture surfaces, that SCC involves discontinuous, brittle fracture [1]. The segregation of magnesium to grain boundaries is possibly also important, e.g. magnesium–hydrogen complexes [6] or thin films of magnesium hydride [5] could be formed. However, neither the precise role of hydrogen nor the precise mechanism of crack growth have been definitely established for intercrystalline SCC.

For transcrystalline SCC in Al–Zn–Mg single crystals, where complications such as

0022–2461/85 $03.00 + .12

magnesium segregation, and grain-boundary structure are not involved, the mechanism of SCC is more easily elucidated. Recent studies [12, 13] have indicated that *adsorbed* hydrogen rather than dissolved hydrogen is responsible since (a) embrittlement was not observed in specimens cathodically charged with hydrogen prior to testing in inert environments, (b) "brittle" crack growth in aqueous environments was observed at crack velocities as high as $\sim 10\,\text{mm sec}^{-1}$ when hydrogen diffusion would not have time to occur, and (c) fracture surfaces produced by SCC were remarkably similar to those produced by adsorption-induced liquid-metal embrittlement (LME). The characteristics of "brittle" transcrystalline cracking, namely extensive slip on planes intersecting cracks, crack growth in $\langle 1\,1\,0\rangle$ directions (on macroscopic $\{1\,0\,0\}$ planes), and small dimples/tear ridges on fracture surfaces, suggested that fracture occurred by localized plastic flow rather than by decohesion. It was therefore proposed [12, 13] that adsorbed hydrogen facilitated the nucleation of dislocations at crack tips and thereby promoted the coalescence of cracks with voids ahead of cracks.

The mechanism proposed for transcrystalline SCC could also be applicable to intercrystalline SCC and this possibility was explored in the present work by determining (a) whether the characteristics of intercrystalline SCC and LME were similar, (b) whether intercrystalline embrittlement in aqueous environments could occur at high crack velocities, (c) whether hydrogen charging prior to testing in inert environments produced embrittlement, and (d) whether significant, localized plasticity and nucleation of voids ahead of cracks were associated with SCC. Bicrystals of a high-purity Al–Zn–Mg alloy, with grain boundaries normal to the stress axis, were used. The metallographic and fractographic characteristics of crack growth for given environments and conditions are relatively uniform for bicrystals compared with polycrystals, and hence can be confidently used to elucidate mechanisms of fracture.

2. Experimental details

2.1. Preparation of bicrystal specimens

Large grains (~ 10 to 30 mm) were grown in high-purity Al–6.27Zn–2.94Mg (~ 0.005 Fe, ~ 0.004 Si) wt% alloy strips by strain-annealing, as described previously [12]. Specimens (40 mm × 10 mm × 2 mm) were cut from the strips such that a centrally located grain boundary was normal to the specimen axis and traversed the entire cross-section. Specimens were centrally notched (~ 1 mm deep) at one edge to facilitate crack initiation at the boundary and then heat-treated.

2.2. Heat treatment and microstructure

Specimens were solution-treated in salt at 450° C for 1 h and then given one of the following treatments:

Treatment A: quenched into boiling water, aged in oil at 100° C for 3 min and then in salt at 180° C for 3 h.

Treament B: quenched into water at 20° C and then aged in oil at 120° C for 24 h.

Treatment C: quenched into water at 20° C and then aged in oil at 90° C for 11 days.

Treatment A results in a low-strength, over-aged condition (Vickers Hardness, $VH_{10} \sim 142$) with a precipitate-free-zone (PFZ) width ~ 170 nm (Fig. 1a). Treatment B results in a peak hardness (T6) condition ($VH_{10} \sim 172$) with a PFZ width ~ 25 nm (Fig. 1b). Treatment C produces an under-aged condition ($VH_{10} \sim 177$) with a PFZ width ~ 15 nm (Fig. 1c). (The "under-aged" condition has a higher hardness than the "peak-hardness" condition since the former was produced by ageing at a lower temperature.) The size and spacing of the grain-boundary precipitates were not quantified but were largest for Treatment A and smallest for Treatment C. Small, widely dispersed inclusions were also present throughout the microstructure.

2.3. Environments

Specimens were tested in dry air, produced by packing magnesium perchlorate or silica gel around specimens, at $\sim 20°$ C, distilled water at $\sim 20°$ C, and a low-melting point (47° C) bismuth alloy (44.7Bi, 22.6Pb, 19.1In, 8.3Sn, 5.3Cd) (wt%) at $\sim 60°$ C. Some specimens (Treatment A) were cathodically charged in 3.5% NaCl plus $250\,\text{mg l}^{-1}$ $NaAsO_2$ at -1.6 V (against SCE) at 20° C for 5 days prior to testing in dry air.

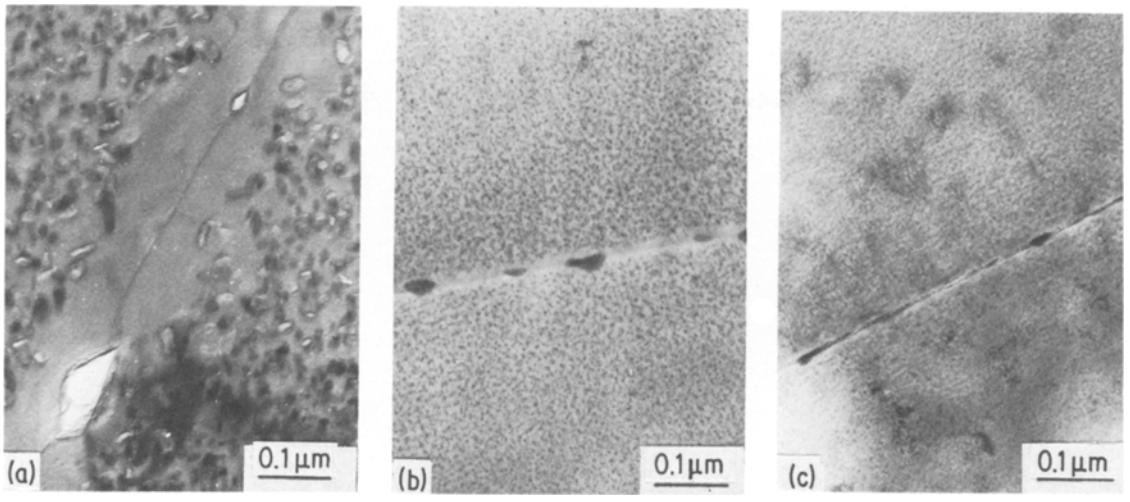

Figure 1 TEM showing microstructures of grain-boundary regions for (a) Treatments A; (b) Treatment B and (c) Treatment C (see Text).

2.4. Testing

Specimens were tested in cantilever or three-point bending under monotonically increasing stress and sustained stress. For the former, specimens were bent rapidly ($\sim 5° \text{sec}^{-1}$) or slowly ($\sim 0.0006° \text{sec}^{-1}$) producing crack-growth rates of 5 to 10 mm sec^{-1} and $\sim 6 \times 10^{-5}$ mm sec^{-1}, respectively. The rates were determined from observations on the polished side surfaces of specimens.

2.5. Examination of specimens

Fracture surfaces were examined by scanning electron microscopy (SEM) and transmission electron microscopy (TEM) of secondary carbon replicas. Observations of LME fractures necessitated removing the bismuth alloy by dissolution in concentrated nitric acid; this treatment did not produce any attack on the underlying aluminium fracture surface. Plastic zones associated with SCC and LME (for Treatments B and C) were revealed in specimen interiors by ageing at 200° C for 30 min after crack growth (thereby producing coarse precipitation on dislocations), then sectioning, polishing, and etching.

3. Results

3.1. Treatment A – low strength, wide PFZ specimens

3.1.1. LME and fracture in dry air

Application of the liquid-alloy environment to the notch region of specimens loaded to just below the stress required for overload fracture in air resulted in immediate, rapid (~ 10 mm sec^{-1}) sub-critical crack growth. When only a small amount of liquid alloy was applied, cracks ran out of the liquid alloy and stopped; specimens were then fractured in dry air. A transition from a "brittle" intercrystalline LME fracture surface to a "ductile" intercrystalline overload fracture surface was then observed (Fig. 2). A larger amount of deformation and lateral contraction on the side surfaces of specimens were also apparent for the overload fractures compared

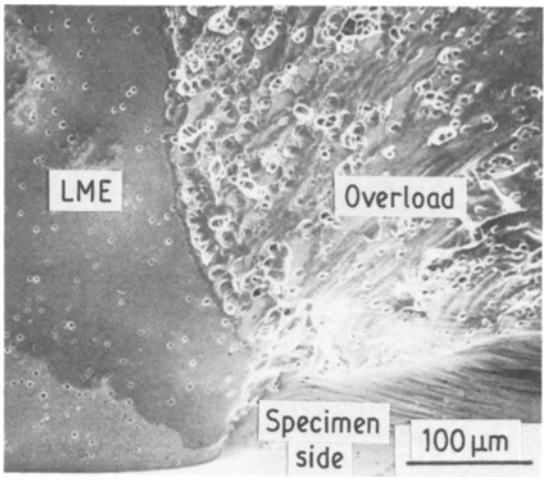

Figure 2 SEM of fracture surface for Treatment A showing transition from LME to overload in air. Note the change in fracture-surface appearance and the larger amount of lateral contraction of the specimen side for overload compared with LME.

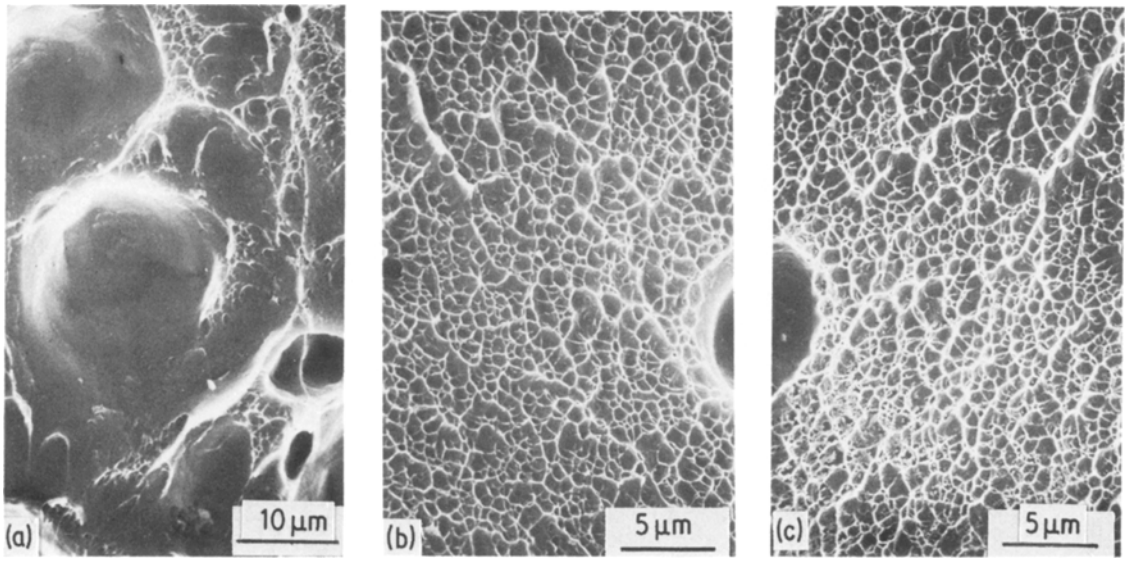

Figure 3 SEM of (a) overload region and (b), (c) mating halves of LME region, as in Fig. 2 but at higher magnifications to show the differences in dimple appearance for LME and overload fractures.

with the LME fractures (Fig. 2). At high magnifications, SEM showed that overload fracture surfaces were covered with large, deep dimples with smaller, shallower dimples between and within the large dimples (Fig. 3a). In contrast, the LME fracture surfaces were covered with small, shallow dimples and isolated large dimples. Examination of stereoscopic pairs of micrographs from mating areas of opposite LME fracture surfaces (Fig. 3b) showed that the dimples were generally equiaxed with dimples on one fracture surface matching those on the other, as would be expected if the dimples resulted from a microvoid-coalescence process.

3.1.2. Rapid fracture in water

The appearance of fracture surfaces of specimens cracked rapidly (5 to 10 mm sec^{-1}) in water was often quite different to that produced by crack growth in dry air. In dry air, large, deep dimples were observed as described above, while small, shallow dimples similar to those produced by LME were observed after fracture in water (Fig. 4). Specimens were cut from the same bicrystal, and hence the differences must be associated with an environmental effect.

3.1.3. SCC in water

Immersion of specimens, loaded to just below

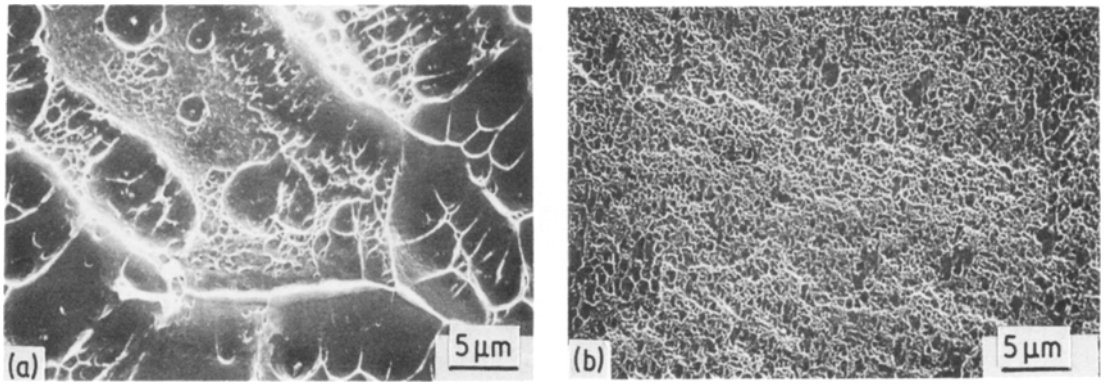

Figure 4 SEM of fracture surface for Treatment A produced by rapid cracking in (a) dry air, and (b) water. Note the difference in appearance of dimples.

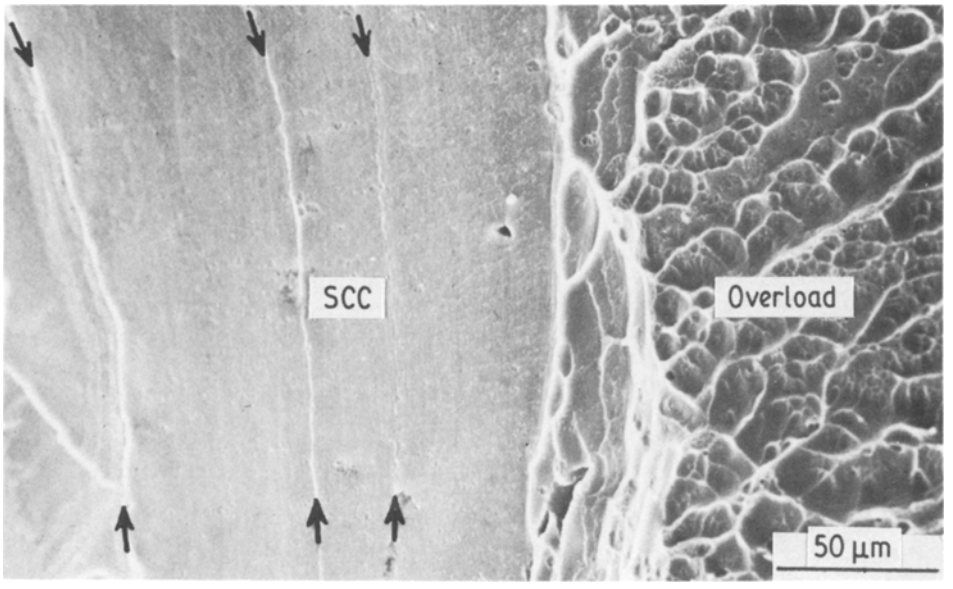

Figure 5 SEM of fracture surface for Treatment A showing transition from SCC at high K to overload in air; note striations (arrowed) on SCC region.

the stress required for overload fracture, in distilled water resulted in sub-critical crack growth with velocities $\sim 10^{-4}$ mm sec^{-1}; after several millimetres of crack growth had occurred, specimens were dried and then fractured in dry air. Transitions from "brittle" intercrystalline SCC fracture surfaces to "ductile" intercrystalline overload fracture surfaces were observed (Fig. 5), as for LME-to-overload fractures. Striations were sometimes observed on SCC fractures (Fig. 5) and were probably crack-arrest markings since striations on one fracture surface matched striations on the other fracture surface. At high magnifications, SEM showed that SCC fractures were covered with small, shallow dimples, similar to those observed on LME fractures (Fig. 6a).

Dimples on SCC (and LME) fractures were only clearly observed after crack growth at high stress intensity factor (K) values – dimples

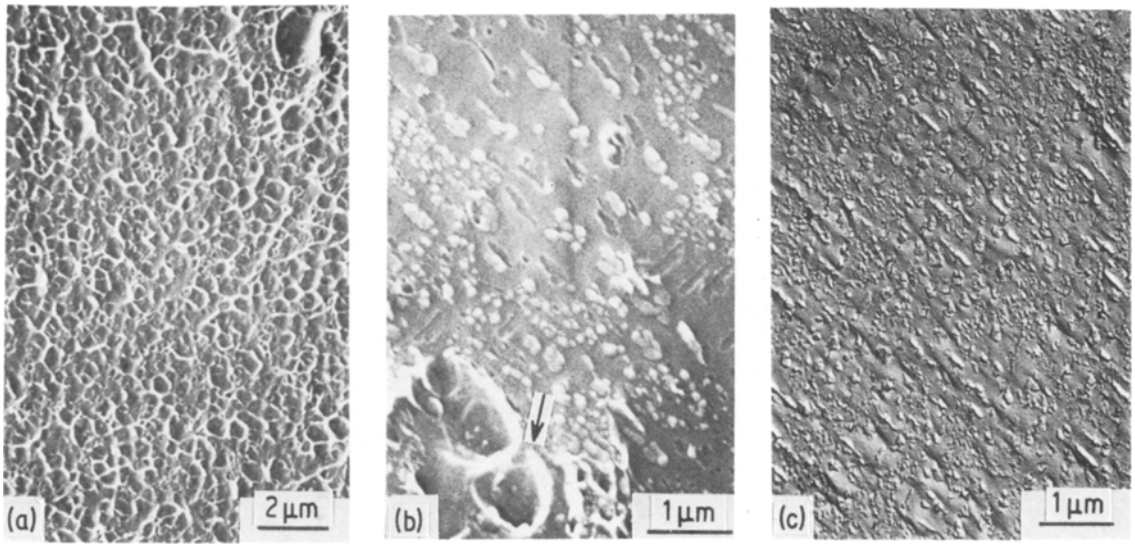

Figure 6 Fracture surfaces produced by SCC for Treatment A (a) at high K showing dimples, (b) at low K showing only isolated dimples (arrowed) using SEM, and (c) at low K showing extremely shallow dimples using TEM.

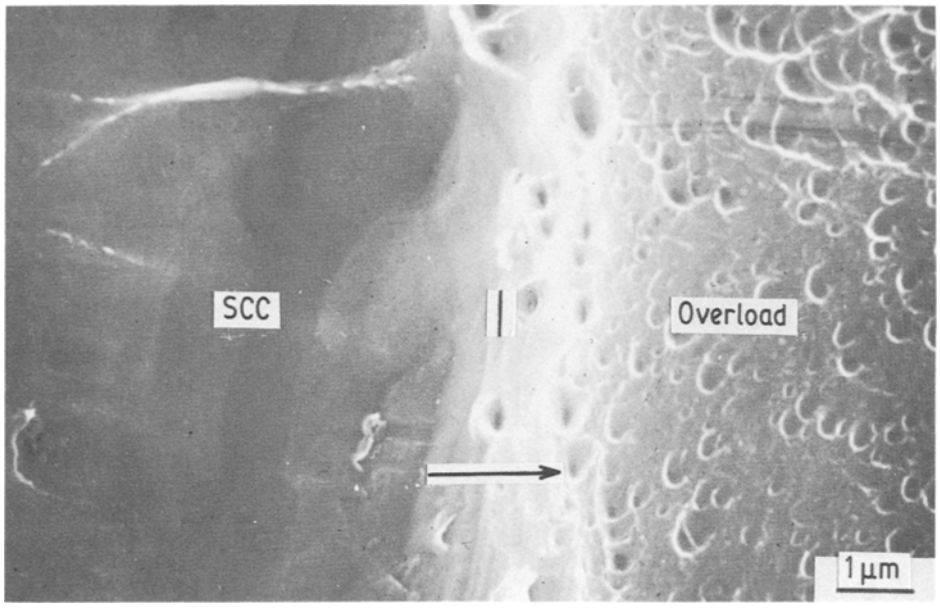

Figure 7 SEM of fracture surface for Treatment B showing transition from smooth SCC fracture produced at high K to dimpled overload fracture.

become shallower and more difficult to resolve with decreasing K. At low K values, SEM revealed relatively smooth fracture surfaces except for precipitates (and precipitate sites) and isolated dimples (Fig. 6b). However, TEM of replicas shadowed at low angles and examined at high tilt angles to enhance contrast, showed that extremely shallow dimples were generally present (Fig. 6c).

3.1.4. Hydrogen-charged specimens

Fracture surfaces of specimens (cut from the same bicrystal) fractured rapidly or slowly in dry air with and without prior cathodic charging were covered with large, deep dimples, i.e. hydrogen charging did not result in embrittlement for Treatment A.

3.2. Treatments B and C – high strength, narrow PFZ specimens

For Treatment B, changing from the liquid alloy or distilled water environment to dry air during crack growth resulted in changes from a "brittle" to a "ductile" fracture-surface appearance (Fig. 7), as observed for Treatment A. However, for Treatment B, overload fractures in dry air were dimpled on a much finer scale than for Treatment A, and dimples were not observed on SCC or LME fracture surfaces. Observations on the polished side surfaces (Fig. 8a) and in the interior (Fig. 8b) of cracked specimens showed that significant plasticity was associated with SCC and LME, although plastic zones were smaller than those associated with overload fractures.

For Treatment C, SEM and TEM of overload fractures produced in dry air generally showed smooth fracture surfaces except for precipitates and slip lines (Fig. 9a), although extremely small, shallow dimples were observed by TEM in some areas (Fig. 9b). SCC and LME fracture surfaces appeared the same as those for Treatment B, i.e. fractures were flat with no evidence of dimples.

4. Discussion

4.1. Mechanism of fracture in dry air

It is well established [14, 15] that intercrystalline fracture of high-strength Al–Zn–Mg alloys in inert environments (*without* prior exposure to hydrogen-bearing environments) involves (a) preferential plastic deformation in soft PFZ adjacent to grain boundaries, (b) nucleation of voids by separation of grain-boundary-precipitate/matrix interfaces, and (c) growth and coalescence of voids. Fracture surfaces are therefore dimpled and the size of dimples

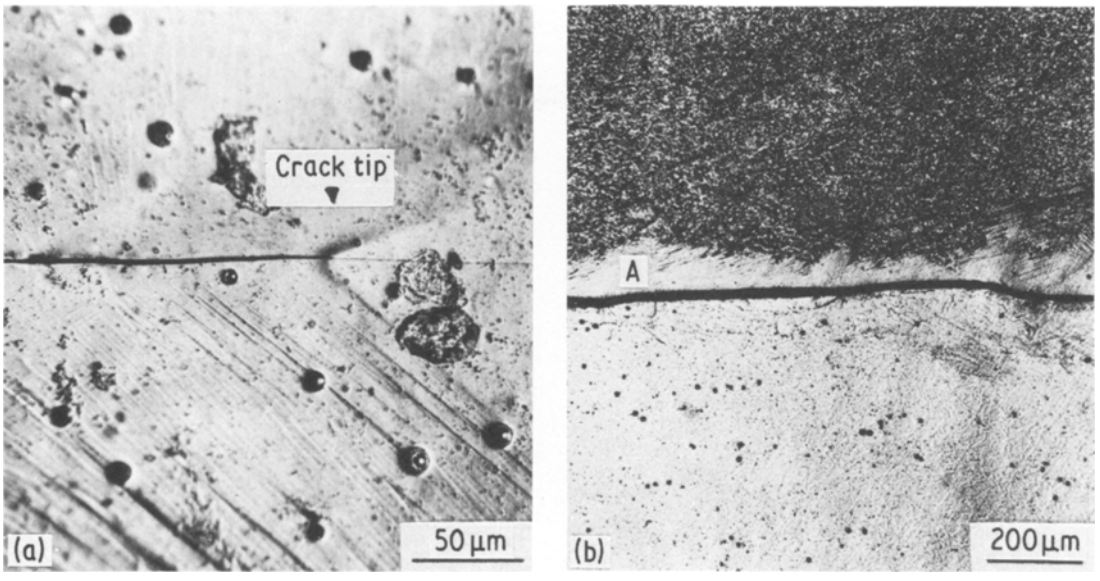

Figure 8 Optical micrographs showing deformation associated with SCC for Treatment B (a) on specimen side, and (b) in specimen interior revealed by ageing after SCC, sectioning, polishing and etching; the light etching zone (A) in the upper grain indicates that considerable deformation has occurred.

depends particularly on the size and spacing of grain-boundary precipitates. The matrix strength (which determines the degree of strain localization in PFZ), the width of PFZ, and the orientation of grain-boundary planes to the tensile-stress direction can also influence the appearance of dimples.

When grain-boundary precipitates are widely spaced, PFZ are wide and matrix strengths are low (as for Treatment A) large, deep dimples are observed on fracture surfaces. Nucleation and growth of voids occurs preferentially around larger precipitates or inclusions and the coalescence of the resulting large voids with each other and with the crack tip then involves nucleation and growth of voids around smaller

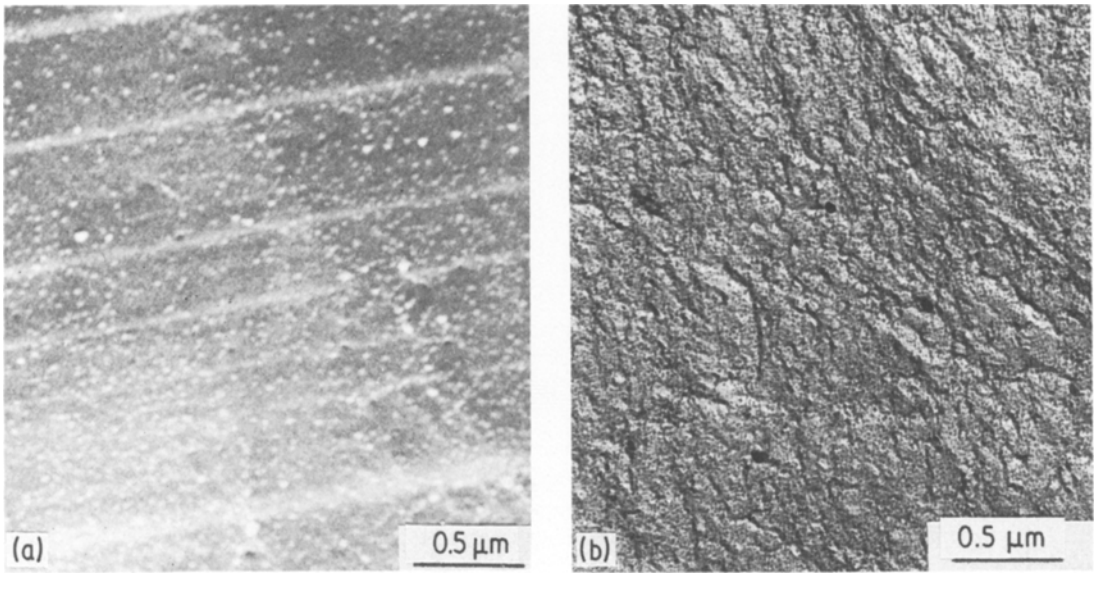

Figure 9 (a) SEM, and (b), TEM of overload fracture surface for Treatment C. SEM shows smooth areas except for precipitate marks and slip lines. TEM reveals areas of extremely shallow dimples.

precipitates. Thus, small dimples are often observed within and around the large dimples. As would be expected, dimples are smaller and shallower when either the spacings of grain-boundary precipitates are smaller, matrix strengths are higher, or PFZ are narrower (or all three, as for Treatments B and C). For Treatment C, fracture-surface dimples were just visible in some areas but not in others suggesting that the microvoid-coalescence process can occur on such a localized scale that dimples are too small and shallow to be replaced by either SEM or TEM fractograph techniques.

4.2. Mechanism of LME

It is generally accepted [16, 17] that rapid subcritical crack growth in liquid-metal environments is associated with *adsorption* of liquid-metal atoms at crack tips. The range of influence of adsorption on metals is only one or two interatomic distances, and hence it is also generally accepted that adsorption reduces the strength of interatomic bonds exactly at crack tips. For Treatment A, LME fracture surfaces were covered with shallower dimples than those on overload fractures, indicating that crack growth in the liquid-metal environment occurred by a more localized microvoid-coalescence process than that in dry air. Similar observations have been made for transcrystalline LME in Al–Zn–Mg, and for LME in other ductile materials [18, 19], and have been explained on the basis that adsorption facilitates the nucleation of dislocations and thereby promotes the coalescence of cracks with voids.

For Treatments B and C, LME fracture surfaces were apparently smooth except for precipitates, and hence crack growth could possibly occur by adsorption-induced decohesion. On the other hand, LME could occur by a microvoid-coalescence process on such a small scale that dimples are not resolved by fractography, as apparently occurs during overload fracture for Treatment C. The observation that considerable slip occurs in precipitation-hardened grain interiors adjacent to LME cracks suggests that strains in soft PFZ are large, and hence that a microvoid-coalescence process is more probable than a decohesion process. Furthermore, the fact that intercrystalline LME occurs at much lower stresses than transcrystalline LME also suggests that crack growth occurs by localized plastic flow; crack growth by decohesion should occur preferentially along a fracture path where there is a minimum of plastic work associated with fracture [20], i.e. across precipitation-hardened grains rather than along soft PFZ at grain boundaries.

4.3. Mechanisms of SCC

Observations that (a) fracture surfaces produced by SCC are similar to those produced by LME, (b) embrittlement in water could occur at high crack velocities for Treatment A, and (c) cathodic charging did not produce embrittlement for Treatment A, all suggest that *adsorbed* hydrogen rather than dissolved hydrogen, hydride films, or dissolution produces intercrystalline SCC. The same three observations and the same conclusion were also made for transcrystalline SCC, as discussed in detail elsewhere [12]. The characteristics of SCC, namely dimpled fracture surfaces for Treatment A and considerable slip adjacent to cracks for Treatments B and C, suggest that SCC occurs by adsorption-induced dislocation nucleation rather than by adsorption-induced decohesion, as discussed for LME.

SCC could sometimes involve other processes besides adsorption, since protective oxide films could form at crack tips and prevent hydrogen adsorption or inhibit dislocation nucleation at crack tips. Diffusion of hydrogen through oxide films and along grain-boundaries ahead of cracks may then be necessary for crack-growth. Fracture of oxides could then produce sudden increments of crack growth if monolayer coverages of hydrogen are present along grain boundaries ahead of cracks, since interatomic bonds at advancing crack tips would be weakened by hydrogen. Alternatively, increments of hydrogen-induced cracking may initiate at grain-boundary precipitates ahead of cracks. Crack growth should stop when the concentration of hydrogen falls below a critical value and the above processes may then be repeated. Such discontinuous cracking should produce crack-arrest markings, as sometimes observed in the present work and by others [1].

Crack advance by decohesion rather than by localized slip could also sometimes occur, since some studies of SCC have not found evidence of slip. For example, studies of SCC in thin foils by TEM [21] showed that crack growth had

occurred along grain boundaries and grain-boundary-precipitate/matrix interfaces; dislocations were not observed and it was suggested that decohesion had occurred. However, dislocations often escape from foils, and hence such evidence is not conclusive.

4.4. Mechanisms of pre-exposure embrittlement

Pre-exposure embrittlement has been observed [2, 8, 22] for under-aged and peak-hardness microstructures but was not observed in the present work or by others [22] for over-aged microstructures. Over-ageing produces coarsening of $MgZn_2$ grain-boundary precipitates and thereby decreases the concentration of elemental magnesium at grain boundaries. Thus, high concentrations of magnesium at grain boundaries are possibly required to produce pre-exposure embrittlement. For example, the presence of magnesium could (a) promote hydrogen adsorption and diffusion along grain boundaries, and (b) favour hydrogen remaining in an embrittling atomic form rather than precipitating at traps as innocuous hydrogen gas. It should also be noted that pre-exposure embrittlement may not be observed if tests are performed at strain rates which are too high or too slow, suggesting that hydrogen diffusion is involved [2, 9]. However, if hydrogen atoms are present at grain boundaries, then they should weaken interatomic bonds at crack tips as discussed for SCC.

Besides the presence of atomic hydrogen at grain-boundaries, pitting and penetration of grain boundaries by hydrated oxide [23] or hydride [7] films could also contribute to pre-exposure embrittlement if corroded surface layers are not removed. Hydrated oxides could provide a source of moisture at crack tips, even when the surrounding atmosphere is nominally dry, so that hydrogen could also be generated during crack growth. The contributions of these effects to pre-exposure embrittlement will depend on the exact experimental procedure and further work is clearly required to determine their relative importance.

5. Conclusions

(a) Crack growth in inert environments occurs by a localized plastic-flow/microvoid-coalescence process in soft PFZ at grain boundaries and produces dimpled fracture surfaces; for very narrow PFZ and high matrix strengths, this process can be so localized that dimples are sometimes not resolved on fracture surfaces.

(b) The metallographic and fractographic observations suggest that both SCC and LME occur by a plastic-flow/microvoid-coalescence process which is more localized than that which occurs in inert environments.

(c) It is proposed that adsorbed hydrogen or liquid-metal atoms weaken interatomic bonds at crack tips, thereby facilitating the nucleation of dislocations and promoting the coalescence of cracks with voids.

Acknowledgement

Part of this work was carried out while the author was a visiting research fellow at the Open University, Milton Keynes, UK, and the support of a Science and Engineering Research Council Grant during this time is gratefully acknowledged.

References

1. G. M. SCAMANS, "Hydrogen Effects in Metals", edited by I. M. Bernstein and A. W. Thompson (Metallurgical Society, AIME, Warrendale, Pennsylvania, USA, 1981) p. 467.
2. N. J. H. HOLROYD and D. HARDIE, "Hydrogen Effects in Metals", edited by I. M. Bernstein and A. W. Thompson (Metallurgical Society, AIME, Warrendale, Pennsylvania, USA, 1981) p. 449.
3. R. E. SWANSON, A. W. THOMPSON, I. M. BERNSTEIN and J. L. MALONEY III, "Hydrogen Effects in Metals", edited by I. M. Bernstein and A. W. Thompson (Metallurgical Society, AIME, Warrendale, Pennsylvania, USA, 1981) p. 459.
4. L. CHRISTODOULOU and H. M. FLOWER, "Hydrogen Effects in Metals", edited by I. M. Bernstein and A. W. Thompson (Metallurgical Society, AIME, Warrendale, Pennsylvania, USA, 1981) p. 493.
5. C. D. S. TUCK, "Hydrogen Effects in Metals", edited by I. M. Bernstein and A. W. Thompson (Metallurgical Society, AIME, Warrendale, Pennsylvania, USA, 1981) p. 503.
6. J. R. PICKENS, D. VENABLES and J. A. S. GREEN, "Hydrogen Effects in Metals", edited by I. M. Bernstein and A. W. Thompson (Metallurgical Society, AIME, Warrendale, Pennsylvania, USA, 1981) p. 513.
7. E. N. PUGH, "Hydrogen Effects in Metals", edited by I. M. Bernstein and A. W. Thompson (Metallurgical Society, AIME, Warrendale, Pennsylvania, USA, 1981) p. 437.
8. G. M. SCAMANS, R. ALANI and P. R. SWANN, *Corros. Sci.* **16** (1976) 443.

9. D. HARDIE, N. J. H. HOLROYD and R. N. PARKINS, *Metal Sci.* **13** (1979) 603.
10. M. O. SPEIDEL, "Hydrogen in Metals", edited by I. M. Bernstein and A. W. Thompson (ASM, Metals Park, Ohio, USA, 1974) p. 249.
11. J. A. S. GREEN, H. W. HAYDEN and W. G. MONTAGUE, "Effect of Hydrogen on Behavior of Materials", edited by A. W. Thompson and I. M. Bernstein (Metallurgical Society, AIME, Warrendale, Pennsylvania, USA, 1975) p. 200.
12. S. P. LYNCH, *Corros. Sci.* **22** (1982) 925.
13. *Idem, ibid.* **24** (1984) 375.
14. P. N. T. UNWIN and G. C. SMITH, *J. Inst. Metals* **97** (1969) 299.
15. T. KAWABATA, H. SUENAGA and O. IZUMI, *J. Mater Sci.* **19** (1984) 1007.
16. M. H. KAMDAR, *Prog. Mater. Sci.* **15** (1973) 289.
17. N. S. STOLOFF, "Atomistics of Fracture", edited by R. M. Latanision and J. R. Pickens (Plenum, New York, 1983) p. 921.
18. S. P. LYNCH, *Acta Metall.* **29** (1981) 325.
19. *Idem, ibid.* **32** (1984) 79.
20. S. S. HECKER, D. L. ROHR and D. F. STEIN, *Metall. Trans.* **9A**(1978) 481.
21. L. MONTGRAIN and P. R. SWANN, "Hydrogen in Metals", edited by I. M. Bernstein and A. W. Thompson (ASM, Metals Park, Ohio, USA, 1974) p. 575.
22. J. ALBRECHT, I. M. BERNSTEIN and A. W. THOMPSON, *Metall. Trans.* **13A** (1982) 811.
23. G. WASSERMANN, *Z. Metallkunde* **34** (1942) 297.

Received 8 October
and accepted 6 November 1984